Mutations in *PIGU* Impair the Function of the GPI Transamidase Complex, Causing Severe Intellectual Disability, Epilepsy, and Brain Anomalies

Alexej Knaus,[1,9,*] Fanny Kortüm,[2,9] Tjitske Kleefstra,[3,9] Asbjørg Stray-Pedersen,[4,9] Dejan Đukić,[1] Yoshiko Murakami,[5] Thorsten Gerstner,[6] Hans van Bokhoven,[3] Zafar Iqbal,[3,7] Denise Horn,[8] Taroh Kinoshita,[5] Maja Hempel,[2,10] and Peter M. Krawitz[1,10]

The glycosylphosphatidylinositol (GPI) anchor links over 150 proteins to the cell surface and is present on every cell type. Many of these proteins play crucial roles in neuronal development and function. Mutations in 18 of the 29 genes implicated in the biosynthesis of the GPI anchor have been identified as the cause of GPI biosynthesis deficiencies (GPIBDs) in humans. GPIBDs are associated with intellectual disability and seizures as their cardinal features. An essential component of the GPI transamidase complex is PIGU, along with PIGK, PIGS, PIGT, and GPAA1, all of which link GPI-anchored proteins (GPI-APs) onto the GPI anchor in the endoplasmic reticulum (ER). Here, we report two homozygous missense mutations (c.209T>A [p.Ile70Lys] and c.1149C>A [p.Asn383Lys]) in five individuals from three unrelated families. All individuals presented with global developmental delay, severe-to-profound intellectual disability, muscular hypotonia, seizures, brain anomalies, scoliosis, and mild facial dysmorphism. Using multicolor flow cytometry, we determined a characteristic profile for GPI transamidase deficiency. On granulocytes this profile consisted of reduced cell-surface expression of fluorescein-labeled proaerolysin (FLAER), CD16, and CD24, but not of CD55 and CD59; additionally, B cells showed an increased expression of free GPI anchors determined by T5 antibody. Moreover, computer-assisted facial analysis of different GPIBDs revealed a characteristic facial gestalt shared among individuals with mutations in *PIGU* and *GPAA1*. Our findings improve our understanding of the role of the GPI transamidase complex in the development of nervous and skeletal systems and expand the clinical spectrum of disorders belonging to the group of inherited GPI-anchor deficiencies.

The linkage of over 150 different proteins to the cell surface is facilitated by the glycosylphosphatidylinositol (GPI) anchor. GPI-anchored proteins (GPI-APs) play important roles in embryogenesis, neurogenesis, signal transduction, and various other biological processes in all tissues of the human body.[1,2] Hence, biosynthesis, modification, and transfer of the GPI anchor to the proteins are highly conserved processes mediated by at least 31 genes. The GPI transamidase is a heteropentameric complex (encoded by *PIGK* [MIM: 605087], *PIGS* [MIM: 610271], *PIGT* [MIM: 610272], *GPAA1* [MIM: 603048], and *PIGU* [MIM: 608528, RefSeq accession number NM_080476.4]) that mediates the transfer of the protein to the GPI anchor in the endoplasmatic reticulum (ER).

A recent protein-sequence analysis study showed that the ten predicted transmembrane domains (TMs) of PIGU share high sequence similarity with the mannosyltransferases PIGM, PIGV, PIGB, and PIGZ but lack functionally important motifs.[3] These ten TMs were anticipated to bind the GPI lipid anchor. In addition, it was determined that PIGU is the last component that associates with the core protein complex of the GPI transamidase formed by PIGT, PIGS, PIGK, and GPAA1.[4] Therefore, the presumed molecular function of PIGU is the presentation of the GPI lipid anchor to the transamidase complex in a productive conformation.[3]

Mutations in three genes of the GPI transamidase complex have been associated with human disease. Severe intellectual disability, global developmental delay, muscular hypotonia, seizures, and cerebellar atrophy were described in individuals with *GPAA1* (GPIBD15 [MIM: 617810])[5] and *PIGT* mutations (GPIBD7 or multiple congenital anomalies-hypotonia-seizures syndrome 3 [MCAHS3 (MIM: 615398)]);[6] *PIGS* deficiency leads to severe global developmental delay, seizures, hypotonia, ataxia, and dysmorphic facial features (GPIBD18 [MIM: 618143]).[7] Here, we describe five individuals from three unrelated families with rare biallelic missense mutations in *PIGU* presenting with global developmental delay, severe-to-profound intellectual disability, muscular hypotonia, seizures, brain anomalies, scoliosis, and mild facial dysmorphism consistent with GPI biosynthesis deficiencies (GPIBDs).[8,9] We provide clinical and functional evidence for a form of a severe autosomal-recessive GPIBD caused by pathogenic mutations in *PIGU*.

[1]Institute for Genomic Statistics and Bioinformatics, University Hospital Bonn, Rheinische Friedrich-Wilhelms-Universität Bonn, 53127 Bonn, Germany; [2]Institute of Human Genetics, University Medical Center Hamburg-Eppendorf, 20246 Hamburg, Germany; [3]Department of Human Genetics, Radboud University Medical Center, 6500 HB Nijmegen, the Netherlands; [4]Norwegian National Unit for Newborn Screening, Division of Pediatric and Adolescent Medicine, Oslo University Hospital, 0424 Oslo, Norway; [5]Research Institute for Microbial Diseases and World Premier International Immunology Frontier Research Center, Osaka University, Suita, Osaka 565-0871, Japan; [6]Department of Pediatrics, Sørlandet Hospital, 4838 Arendal, Norway; [7]Department of Neurology, Oslo University Hospital, 0424 Oslo, Norway; [8]Institute of Medical and Human Genetics, Charité-Universitätsmedizin Berlin, 13353 Berlin, Germany
[9]These authors contributed equally to this work
[10]These authors contributed equally to this work
*Correspondence: knausa@uni-bonn.de
https://doi.org/10.1016/j.ajhg.2019.06.009.

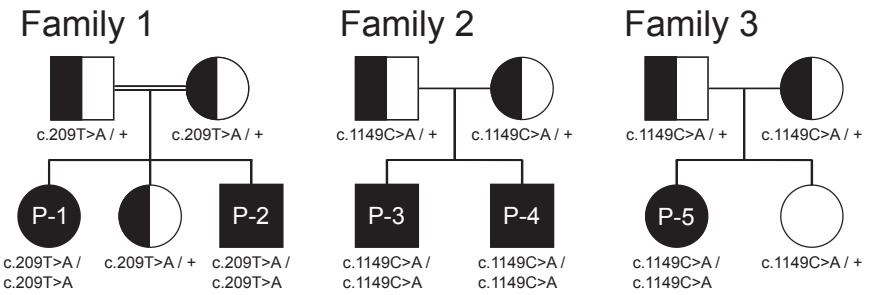

Figure 1. Pedigrees of the Families 1, 2, and 3 with the Mutations in *PIGU*
The consanguineous parents from family 1 are of Turkish descent. Family 2 is from the Netherlands. Family 3 is from Norway.

Proband P-1 was the first daughter of healthy first-degree cousins (family 1) from Turkey; she was born at term after an uncomplicated pregnancy. Myoclonic seizures occurred within the first months and responded poorly to treatment. At the age of 7 months, a global developmental delay and severe muscular hypotonia with reduced spontaneous movements were noted. Magnetic resonance imaging (MRI) of her brain revealed delayed myelination and a small focal periventricular gliosis on the left side. Persistent focal myoclonic seizures, occurrence of generalized myoclonic-tonic seizures, and spasticity in all limbs led to a slow regression and loss of all achieved skills. Repeated MRI of her brain at the ages of 4 years and 12 years showed atrophy of the white matter. When we saw her at the age of 19 years, we saw a profoundly disabled young woman with poor interaction and without speech; she was wheelchair bound and fed by a gastric tube. X-rays of her spine revealed osteopenia and scoliosis (See case reports in Supplemental Data).

Her brother (P-2) was the third child of family 1 and was born at term after a normal pregnancy. At age 7 weeks, the first generalized seizure occurred, followed by a series of therapy-resistant frequent focal myoclonic seizures. He showed profound developmental delay, muscular hypotonia, and poor eye contact. Visual evoked cortical potentials (VECPs) were absent on the right eye and diminished on the left eye. An electrocardiogram (ECG) revealed an incomplete right bundle branch block (RBBB), and echocardiography showed an atrial septal defect (ASD) type II. At the age of 4 years, he had supraventricular tachycardia followed by further episodes requiring hospitalization and cardioversion. When we saw him at the age of 12 years, we saw a wheelchair-bound boy with profound intellectual disability, poor interaction, no speech, and severe scoliosis and who was fed by a percutaneous endoscopic gastrostomy (PEG) tube.

P-3 is the first son of non-consanguineous healthy parents of European descent (family 2); he was born at 42 weeks of gestation after a normal pregnancy. He was hypotonic but without feeding problems. At the age of 11 months, he developed mainly myoclonic seizures and absences that were treated but not fully controlled. A brain MRI showed progressive cerebellar atrophy. At the age of 6 years, he showed a dysmetric movement disorder and profound developmental delay. Scoliosis was surgically corrected at the age of 17 years.

His brother (P-4) was born at term after a normal pregnancy. He was hypotonic. Brain MRI performed at the age of 4 months showed frontal atrophy and a Dandy Walker variant. His global development was profoundly delayed; he was able to speak two-to-three-word sentences and to walk a few steps at age of 5 years. At the age of 6 years, myoclonic epilepsy developed; this is now well controlled. An MRI done at this age showed progressive vermis hypoplasia. At his current age of 12 years, he is able to walk independently for short distances and to speak sentences of a few words. He has also developed scoliosis.

P-5 was the first daughter born to non-consanguineous healthy parents from Norway (family 3); she was born at 42 weeks of gestation after a normal pregnancy. She was hypotonic and had feeding problems. A brain MRI performed at the age of 10 months showed a thin corpus callosum and an enhanced ventricular system without signs of hydrocephalus. Her global development was profoundly delayed. Focal myoclonic seizures started at 3.5 years of age and were responding well to therapy. When we saw her at 5 years of age, she was a wheelchair-bound girl who spoke only few words and had impaired cortical vision. She was considered for a surgical correction of her scoliosis.

The individuals in this study were identified via the MatchmakerExchange platform[10] using data that originated from the University Medical Center Hamburg-Eppendorf, Germany (family 1, P-1 and P-2), the Radboud University Hospital, Nijmegen, the Netherlands, (family 2, P-3 and P-4) and the Norwegian National Unit for Newborn Screening, Division of Pediatric and Adolescent Medicine, Oslo, Norway (family 3, P-5). All samples were obtained after written informed consent was given by the guardians of the affected individuals. The study was performed in accordance with the Declaration of Helsinki protocols and approved by the ethics committees of the respective institutions.

Whole-exome sequencing (WES) revealed two rare homozygous variants in *PIGU* (GenBank: NM_080476.4): c.209T>A (p.Ile70Lys), exon 3 in the two affected siblings (P-1 and P-2) of family 1, and c.1149C>A (p.Asn383Lys), exon 11 in families 2 and 3 (Figures 1 and 2A). Sanger sequencing confirmed biparental inheritance of the variants in all families; pedigrees and genotypes are shown in Figure 1. The variant c.209T>A (CADD score 25.9) has not been observed in gnomAD,[11] while c.1149C>A (CADD score 26.5) has been observed only in a heterozygous state, in individuals from a European population, and with an allele frequency of 7/277194. Both variants

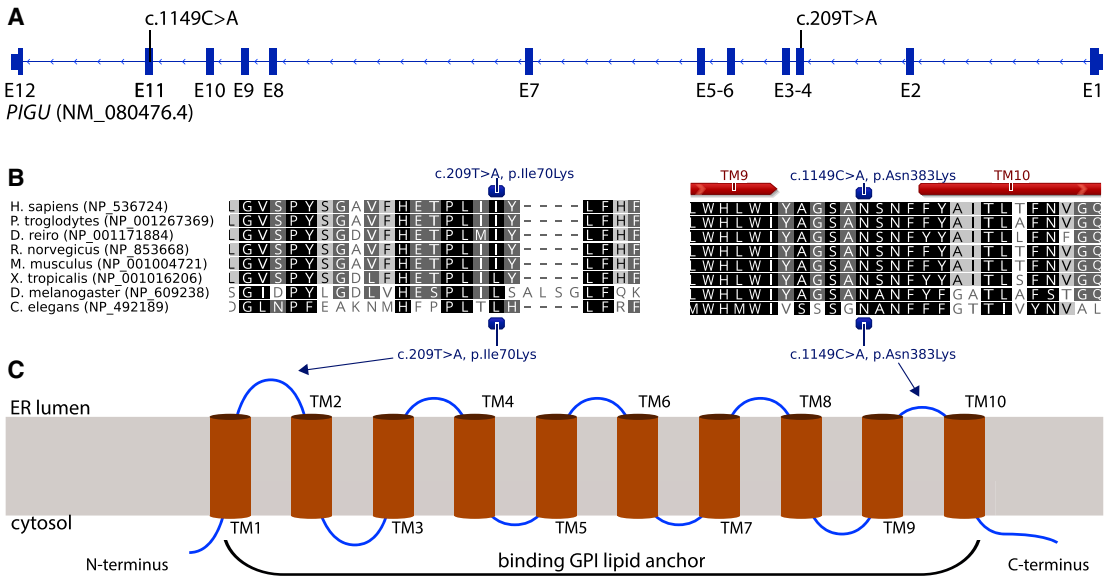

Figure 2. Position of Mutations in *PIGU* Gene and Protein
(A) Exon-intron structure and mutational landscape of *PIGU*.
(B) Conservation (black to gray shading) of PIGU protein sequence over multiple species and prediction of transmembrane (red arrows) domains.
(C) Transmembrane domain structure and location of missense variants in PIGU.

were predicted to be pathogenic by MutationTaster,[12] UMD Predictor,[13] SIFT,[14] and PolyPhen2.[14] The exchange of the hydrophobic amino acid isoleucine at position 70 to a hydrophilic lysine was predicted to cause a conformational change of the first ER luminal domain between TM1 and TM2 (Grantham score 102). The exchange of the amino acid asparagine to lysine at position 383 is also positioned in an ER luminal domain before TM10 (Grantham score 94) (Figures 2B and 3C).

To assess the functional implications of the missense variants in *PIGU* for the GPI anchoring process, we performed flow cytometry on peripheral blood samples collected in CytoChex blood collection tubes (BCTs). For multicolor flow cytometry, cells were stained with fluorescently labeled antibodies against GPI-APs (CD16, CD24, CD55, and CD59), as well as with fluorescein-labeled proaerolysin (FLAER), which binds to the GPI anchor itself. Use of the T5 4E10 antibody allowed detection of free GPI anchors.[15–18]

Relative reduction of GPI-AP was calculated as a ratio of the staining index (SI) of an affected individual to the SIs of healthy parents and healthy unrelated controls. It is noteworthy that there were only subtle differences in GPI-AP staining between heterozygous carriers of pathogenic mutations (parents) and unrelated healthy controls.

As revealed by reduced expression of FLAER, the relative expression of GPI-APs CD16 and CD24 was significantly reduced on granulolcytes compared to controls. But CD55 expression was not significantly altered and CD59 expression was only slightly increased in three out of four individuals with mutations in *PIGU* compared to controls. (Figure 3). However, CD55 expression was not altered from that of controls, whereas CD59 expression was higher than that in controls in three out of four individuals with mutations in *PIGU*. This characteristic pattern of marker staining was observed in some individuals with mutations in *PIGT*, but this was not addressed by the authors.[19,20] The deficiency of the GPI transamidase in linking GPI-APs to the GPI anchor results in an abundance of free GPI on the cell surface. This can be assessed by the T5 antibody, which binds to the N-acetyl-galactoseamine side branch at the first mannose of the GPI anchor.[16,21] Compared to that of controls, the MFI for T5 of affected individuals' B cells (for monocytes and granulocytes, data not shown) showed an increase of up to 3-fold (Figure 3). Thus, we conclude that the identified missense mutations in *PIGU* reduce the function of the GPI transamidase complex and lead to accumulation of free GPI anchor on the cell surface. Functional validation of the p.Asn383Lys variant was performed in a CHO cell line deficient for *PIGU*. Expression of GPI-APs was rescued less efficiently by transient expression of the p.Asn383Lys mutant than by wild-type *PIGU* (Figure S3).

In order to analyze the phenotypic spectrum of the GPI transamidase deficiency and compare it to other GPIBDs, we conducted a systematic review of the phenotypic features of the most prevalent GPIBDs from the literature and additional cases with molecularly diagnosed GPIBDs (unpublished data). Therefore, we included individuals with mutations in *PIGT* (n = 26), *GPAA1* (n = 10), *PIGU* (n = 5), and *PIGS* (n = 4, excluding two fetuses) for the GPI transamidase deficiencies; *PIGV* (n = 26) and *PGAP3* (n = 28) for two types of hyperphosphatasia with mental retardation syndrome (HPMRS), HPMRS1 (MIM: 239300)

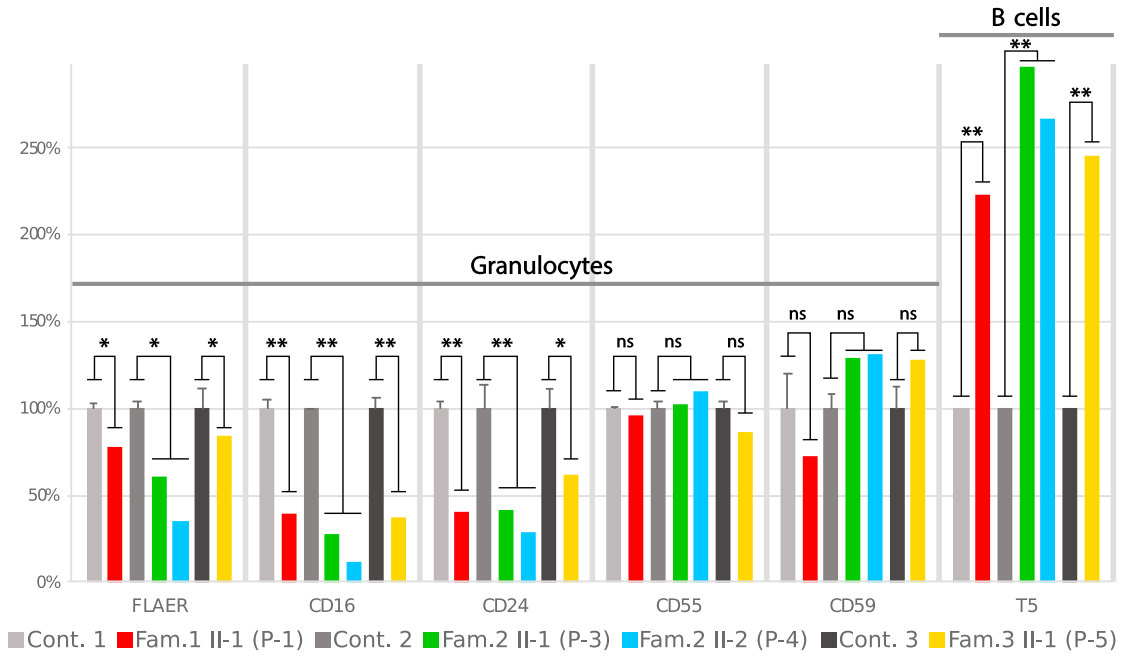

Figure 3. Relative Cell Surface Expression of GPI-APs on Granulocytes and B Cells
On granulocytes of affected individuals (P-1, P-3, P-4, and P-5) a significant relative reduction of cell surface expression of FLEAR, CD16, and CD24 was observed compared to controls. But expression of CD55 and CD59 was not significantly altered on granulocytes. An increased expression of free GPI anchors was detected based on the presence of T5 antibody on B cells in affected individuals compared to controls. Values represent mean + SD. Error bars: n = 3 (parents and one healthy unrelated control), significance was verified by Student's t-test, ns = not significant, *p<0.05, **p<0.01.

and HPMRS3 (MIM: 615716), respectively; and *PIGN* (n = 30; MIM: 606097) and *PIGA* (n = 54; MIM: 311770) for two types of multiple congenital anomalies-hypotonia-seizures syndrome (MCAHS), MCAHS1 (MIM: 614080) and MCAHS3 (MIM: 300868), respectively. We grouped the reported clinical features of the cases in the following 16 feature classes: developmental delay and/or intellectual disability, muscular hypotonia, seizures, cerebellar anomalies (cerebellar hypoplasia, vermis hypoplasia, etc.), anomalies of the corpus callosum (CC)(including thin CC or hypoplasia of the CC), hearing impairment (including hearing loss), cortical visual impairment

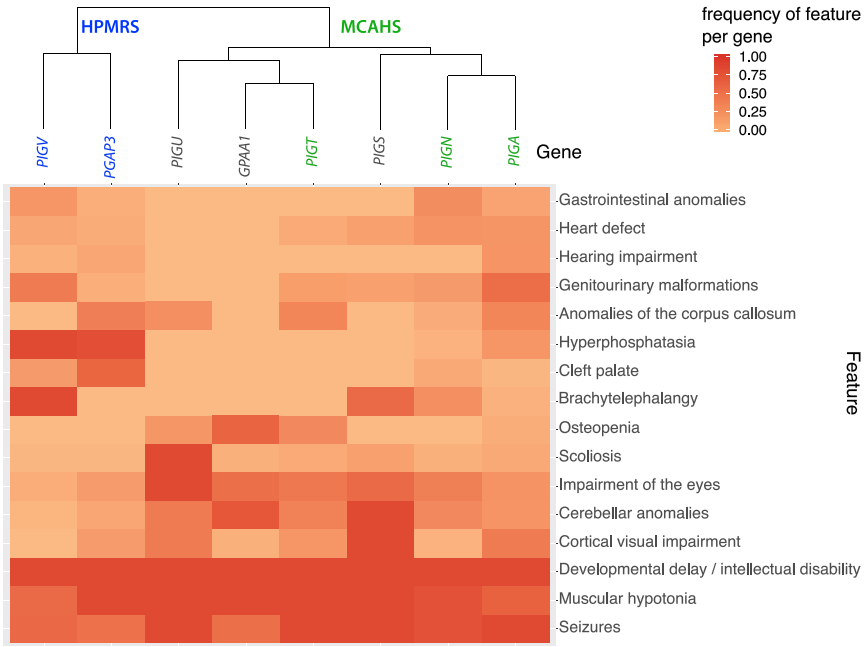

Figure 4. Clustering and Heatmap of Feature Frequency per Gene
Genes of the HPMRS disease entity are highlighted in blue, MCAHS genes in green.

Table 1. Comparison of the Clinical Features of Individuals with Mutations in *PIGU* versus Previously Reported Individuals with Mutations in *PIGT*, *PIGS*, and *GPAA1*

	***PIGU* P-1**	***PIGU* P-2**	***PIGU* P-3**	***PIGU* P-4**	***PIGU* P-5**	***PIGT* (n = 13)**[19,20,22–25]	***PIGS* (n = 6)**[7]	***GPAA1* (n = 10)**[5]
Age	19 years	12 years	17 years	12 years	5 years	11 months to 12 years	prenatal to 5.5 years	4 to 30 years
Measurements	microcephaly	normal	Normal	normal	macrocephaly	microcephaly (2/9, 3 ND)	microcephaly (2/4, 2 ND)	short stature (5/10), microcephaly (1/10)
Alkaline phosphatase	normal	normal	Normal	normal	normal	low 8/13	normal (6/6)	normal (10/10)
Developmental delay	profound	profound	Profound	severe	profound	profound (13/13)	yes (4/4, 2 ND)	mild to moderate (10/10)
Intellectual disability	profound	profound	Profound	severe	profound	profound (13/13)	yes (4/4, 2 ND)	mild to moderate (10/10)
Muscular hypotonia	yes	yes	Yes	yes	yes, severe	yes (13/13)	yes (4/4, 2 ND)	yes (10/10)
Spasticity	yes	yes	no	no	no	ND	no	yes (4/9, 1 ND)
Seizures	yes	yes	Yes	yes	yes	yes (13/13)	yes (4/4, 2 ND)	yes (7/10)
Cerebral atrophy	global	global	no	frontal	mild global	yes (9/11, 2 ND)	yes (2/4, 2 ND)	no
Cerebellar hypoplasia	progressive	no	progressive	progressive	no	yes (9/11)	yes (4/4, 2 ND)	yes (9/10)
Cortical blindness	yes	yes	no	no	yes	yes (9/9)	yes (3/4)	yes (1/10)
Strabismus	yes	yes	yes	yes	yes	yes (9/9)	ND	ND
Nystagmus	no	no	no	no	yes	ND	yes (3/4)	yes (7/10)
Scoliosis	severe	severe	severe	yes	severe	yes (5/7)	yes (1/4)	mild (n = 1)
Osteopenia	yes	ND	ND	ND	ND	yes (7/9)	ND	yes (8/10)
other	slender bones	no	no	no	no	no	brachydactyly (4/6)	no

"ND" indicates not documented.

(including cortical blindness), impairment of the eyes (including strabism, nystagmus, and severe hyper- or myopia), cleft palate, genitourinary anomalies (including malformations of kidneys, urinary tract, or genitalia), heart defects (including ASD and patent ductus arteriosus), scoliosis, osteopenia (including osteoporosis), gastrointestinal anomalies (Hirschsprung disease and megacolon), brachyphalangy (including hypoplastic nails and short fingers or fingertips), and hyperphosphatasia. We counted the phenotypic features and divided by the number of cases that were assessed for each particular feature to determine the feature frequency per gene. The feature frequencies were plotted in a two-dimensional heatmap, and clustering was performed on the basis of Euclidian distance as a measure of similarity.

The feature analysis revealed a high similarity among individuals with mutated genes of the GPI transamidase complex (*GPAA1*, *PIGT*, and *PIGU*); their shared features were cerebellar anomalies, impairments of eyes, and osteopenia. However, osteopenia might be related to the inactivity of these severely disabled people. Scoliosis was identified in nearly all *PIGU*-deficient individuals and is probably a typical clinical feature of *PIGU*-associated GPIBD. So far, hearing impairment and hyperphosphatasia have not been described in individuals with GPI transamidase deficiency. Genitourinary malformations and heart defects without hyperphosphatasia and cleft palate were frequent in individuals with *PIGT*, *PIGN*, and *PIGA* mutations and are therefore considered characteristic for the MCAHS disease entity. Hypophosphatasia and cleft palate (together with brachyphalangy) were the most common features in individuals with *PIGV* and *PGAP3* mutations, and these features represent the major symptoms in HPMRS. The dichotomy between the HPMRS and MCAHS characteristic phenotypic features is visualized in the two branches of the dendrogram in Figure 4. However, delineation of these disease entities based on the frequency of phenotypic features is challenging because of the broad phenotypic variability of MCAHS and also because elevated amounts of serum alkaline phosphatase (ALP) is not restricted to HPMRS. The major discriminatory features between HPMRS and other GPIBDs are increased levels of ALP in combination with cleft palate and brachytelephalangy. Genitourinary malformations were described in most individuals with *PIGV* deficiency, while anomalies of the corpus callosum were identified in most *PGAP3*-affected individuals. Except for in the case of brain

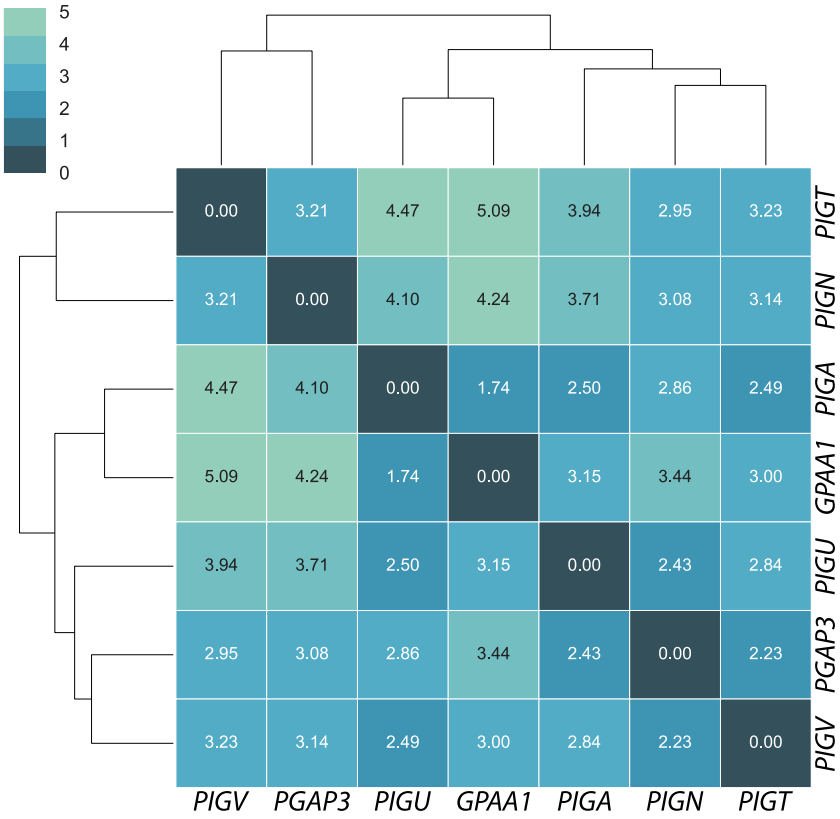

Figure 5. Pairwise Distances of Gene Centroids of Facial Image Embeddings from GPIBD Cases

The FaceNet-based image analysis of 112 molecularly diagnosed GPIBD cases achieved a gene-level classification accuracy of 62%.

anomalies, malformations were more prevalent in individuals with HPMRS than in individuals with the MCAHS spectrum, whereas in the latter group, a higher frequency of brain abnormalities has been documented. Cerebellar anomalies were frequent in all GPIBDs except HPMRS. All individuals with GPIBDs were affected by developmental delay and/or intellectual disability, muscular hypotonia, and seizures. A comparison of the phenotypic features of all diagnosed individuals with mutations in *PIGU* versus those of individuals with mutations in *GPAA1*, *PIGT*, and *PIGS* is presented in Table 1. More comprehensive clinical descriptions are listed in the Supplemental Data.

A characteristic facial gestalt was observed for many individuals with GPIBDs. In a recent study, the facial features of individuals with GPIBDs were analyzed with FDNA's DeepGestalt neural network.[26,27] However, the five individuals with *PIGU* mutations presented with only very subtle characteristic facial features. Therefore, we applied an approach with higher sensitivity and specificity to analyze genotype-phenotype correlations. Here, we used data from previously published cases[5,25,26] as well as unpublished facial images of individuals with mutations in *GPAA1*, *PIGA*, *PIGN*, *PGAP3*, and *PIGT* to compare the facial gestalt to that of individuals with mutations in *PIGU* (n = 5). We chose *PIGA* (n = 25), *PIGN* (n = 15), *PIGT* (n = 13), *PIGV* (n = 24), and *PGAP3* (n = 25) (unpublished data) as the most prevalent GPIBDs and we chose *GPAA1* (n = 5) as another gene of the GPI transamidase complex. In total, 112 molecularly confirmed cases were processed. Informed consent was obtained from all families and was approved by the institutional review boards at the relevant institutions. Embeddings of facial images in a 128-dimensional space were calculated via a FaceNet-based approach.[28] A pairwise distance comparison of the centroids of each gene cohort was then performed and clustered on the basis of Euclidian distances as the measure of similarity (Figure 5). In this approach, we achieved a gene-level classification accuracy of 62%, which is significantly better than random chance (1/7 = 14.3%).

As described previously by Knaus et al.,[26] individuals with *PGAP3* and *PIGV* mutations shared a characteristic facial gestalt and represented the HPMRS branch in the dendrogram (Figure 5). Also, individuals with MCAHS (*PIGN*, *PIGA*, and *PIGT*) shared facial similarities. As a result of shared facial similarities, the five individuals with *PIGU* mutations and the five with *GPAA1* mutations formed a GPI transamidase branch in the dendrogram (Figure 5). It is notable that in our analysis, the facial gestalt of individuals with *PIGT* mutations shows a high level of dissimilarity to those individuals with *PIGU* (distance 2.49) and *GPAA1* (3.00) mutations.

Discussion

Here, we describe a type of the autosomal-recessive GPIBD caused by bi-allelic mutations in *PIGU*. Deep phenotyping of the five affected individuals and of published cases with GPIBDs revealed shared phenotypic features in individuals with mutations in genes of the GPI transamidase complex. Impairment of the nervous system (cortical impairment of vision, cerebellar anomalies, and anomalies of the corpus callosum) with severe motor delay and associated skeletal anomalies (scoliosis and osteopenia) were characteristic in people with GPI transamidase deficiency. Intellectual disability or developmental delay, muscular hypotonia, and seizures are shared features among all individuals with GPIBD.

Computer-assisted facial analysis supported our assumption of facial similarities among individuals with GPI transamidase deficiency (with mutations in *PIGU* and *GPAA1*),

individuals with HPMRS (with mutations in *PIGV* and *PGAP3*), and individuals with MCAHS (with mutations in *PIGA*, *PIGN*, and *PIGT*). We show that the effectiveness of computer-assisted gestalt analysis has a high potential to draw conclusions on the disturbed gene or protein complex in individuals with GPIBDs and probably beyond. We were able to achieve a better-than-random accuracy of 62% in predicting the affected gene in a pathway disorder solely from facial images, in spite of the unbalanced cohorts with few cases and different ethnic backgrounds. Computer-readable information contained in human face permitted classification of phenotypes into disease entities or syndrome families,[26,29–31] and this classification could in turn be used to predict affected genes or identify novel disease genes in known pathways.[32] Moreover, the combination of computer-assisted facial analysis and deep phenotyping might not only be helpful in disease-gene identification but could also improve variant prediction in exome or genome data analysis.

The phenotypic features resulting from functional impairment of *PIGU* were corroborated by flow-cytometric analysis of GPI-AP expression and identification of free GPI anchors on the cell surfaces of blood cells. A biochemical discrimination of GPI transamidase deficiencies and other GPIBDs is possible through use of the T5 4E10 antibody.[18] More importantly, in a functional workup of suspected GPIBDs, a multicolor flow cytometry panel is necessary in order to avoid missing potential GPIBD cases in which expression of several GPI markers is not reduced. Here, we define a multicolor flow cytometry panel (consisting of the GPI markers FLAER, CD16, CD24, CD55, CD59, and T5) to identify a characteristic profile of GPI marker expression in GPI transamidase deficiency. A more detailed and standardized analysis of GPI-AP expression of molecularly confirmed GPIBD cases might potentially identify more gene-specific or protein-complex-specific flow-cytometry profiles.

In conclusion, application of deep phenotyping in combination with computer-assisted facial analysis can support the diagnosis of suspected GPIBD cases where access to sequencing or flow cytometry is limited. Furthermore, this approach can help researchers to interpret variants of unknown clinical significance in GPIBD-associated genes. The identification of more individuals with GPIBDs and deep phenotyping thereof might facilitate prognostication of the condition on the basis of the mutated gene.

Accession Numbers

The mutations in this report have been deposited at www.gene-talk.de and can be accessed at the following URLs: http://www.gene-talk.de/annotations/1371027 and http://www.gene-talk.de/annotations/1371028.

Supplemental Data

Supplemental Data can be found online at https://doi.org/10.1016/j.ajhg.2019.06.009.

Acknowledgments

This work was supported by the Berlin-Brandenburg Center for Regenerative Therapies (BCRT) (Bundesministerium für Bildung und Forschung, project number 0313911). We would like to thank Samuel C.C. Chiang and professor Yenan T. Bryceson at Center for Hematology and Regenerative Medicine, Karolinska University Hospital Huddinge, Stockholm, Sweden for performing the initial flow-cytometry analysis with staining of GPI-linked cell-surface markers in whole blood for the proband P-5 in family 3.

Declaration of Interests

The authors declare no competing interests.

Received: March 7, 2019
Accepted: June 7, 2019
Published: July 25, 2019

Web Resources

GeneTalk, http://www.gene-talk.de
Matchmaker Exchange, https://www.matchmakerexchange.org
Online Mendelian Inheritance in Man, https://www.omim.org

References

1. Kinoshita, T., Fujita, M., and Maeda, Y. (2008). Biosynthesis, remodelling and functions of mammalian GPI-anchored proteins: Recent progress. J. Biochem. *144*, 287–294.
2. Kinoshita, T. (2014). Biosynthesis and deficiencies of glycosylphosphatidylinositol. Proc. Jpn. Acad., Ser. B, Phys. Biol. Sci. *90*, 130–143.
3. Eisenhaber, B., Sinha, S., Wong, W.-C., and Eisenhaber, F. (2018). Function of a membrane-embedded domain evolutionarily multiplied in the GPI lipid anchor pathway proteins PIG-B, PIG-M, PIG-U, PIG-W, PIG-V, and PIG-Z. Cell Cycle *17*, 874–880.
4. Hong, Y., Ohishi, K., Kang, J.Y., Tanaka, S., Inoue, N., Nishimura, J., Maeda, Y., and Kinoshita, T. (2003). Human PIG-U and yeast Cdc91p are the fifth subunit of GPI transamidase that attaches GPI-anchors to proteins. Mol. Biol. Cell *14*, 1780–1789.
5. Nguyen, T.T.M., Murakami, Y., Sheridan, E., Ehresmann, S., Rousseau, J., St-Denis, A., Chai, G., Ajeawung, N.F., Fairbrother, L., Reimschisel, T., et al. (2017). Mutations in GPAA1, encoding a GPI transamidase complex protein, cause developmental delay, epilepsy, cerebellar atrophy, and osteopenia. Am. J. Hum. Genet. *101*, 856–865.
6. Kvarnung, M., Nilsson, D., Lindstrand, A., Korenke, G.C., Chiang, S.C., Blennow, E., Bergmann, M., Stödberg, T., Mäkitie, O., Anderlid, B.M., et al. (2013). A novel intellectual disability syndrome caused by GPI anchor deficiency due to homozygous mutations in PIGT. J. Med. Genet. *50*, 521–528.
7. Nguyen, T.T.M., Murakami, Y., Wigby, K.M., Baratang, N.V., Rousseau, J., St-Denis, A., Rosenfeld, J.A., Laniewski, S.C., Jones, J., Iglesias, A.D., et al. (2018). Mutations in PIGS, encoding a GPI transamidase, cause a neurological syndrome ranging from fetal akinesia to epileptic encephalopathy. Am. J. Hum. Genet. *103*, 602–611.

8. Ng, B.G., and Freeze, H.H. (2015). Human genetic disorders involving glycosylphosphatidylinositol (GPI) anchors and glycosphingolipids (GSL). J. Inherit. Metab. Dis. *38*, 171–178.
9. Jaeken, J., and Péanne, R. (2017). What is new in CDG? J. Inherit. Metab. Dis. *40*, 569–586.
10. Sobreira, N.L.M., Arachchi, H., Buske, O.J., Chong, J.X., Hutton, B., Foreman, J., Schiettecatte, F., Groza, T., Jacobsen, J.O.B., Haendel, M.A., et al.; Matchmaker Exchange Consortium (2017). Matchmaker Exchange. Curr. Protoc. Hum. Genet. *95*, 1–, 15.
11. Lek, M., Karczewski, K.J., Minikel, E.V., Samocha, K.E., Banks, E., Fennell, T., O'Donnell-Luria, A.H., Ware, J.S., Hill, A.J., Cummings, B.B., et al.; Exome Aggregation Consortium (2016). Analysis of protein-coding genetic variation in 60,706 humans. Nature *536*, 285–291.
12. Schwarz, J.M., Cooper, D.N., Schuelke, M., and Seelow, D. (2014). MutationTaster2: Mutation prediction for the deep-sequencing age. Nat. Methods *11*, 361–362.
13. Langmead, B., Trapnell, C., Pop, M., and Salzberg, S.L. (2009). Ultrafast and memory-efficient alignment of short DNA sequences to the human genome. Genome Biol. *10*, R25.
14. Li, M.X., Kwan, J.S., Bao, S.Y., Yang, W., Ho, S.L., Song, Y.Q., and Sham, P.C. (2013). Predicting mendelian disease-causing non-synonymous single nucleotide variants in exome sequencing studies. PLoS Genet. *9*, e1003143.
15. Azzouz, N., Shams-Eldin, H., Niehus, S., Debierre-Grockiego, F., Bieker, U., Schmidt, J., Mercier, C., Delauw, M.F., Dubremetz, J.F., Smith, T.K., and Schwarz, R.T. (2006). Toxoplasma gondii grown in human cells uses GalNAc-containing glycosylphosphatidylinositol precursors to anchor surface antigens while the immunogenic Glc-GalNAc-containing precursors remain free at the parasite cell surface. Int. J. Biochem. Cell Biol. *38*, 1914–1925.
16. Hirata, T., Mishra, S.K., Nakamura, S., Saito, K., Motooka, D., Takada, Y., Kanzawa, N., Murakami, Y., Maeda, Y., Fujita, M., et al. (2018). Identification of a Golgi GPI-N-acetylgalactosamine transferase with tandem transmembrane regions in the catalytic domain. Nat. Commun. *9*, 405.
17. Striepen, B., Tomavo, S., Dubremetz, J.F., and Schwarz, R.T. (1992). Identification and characterisation of glycosyl-inositolphospholipids in Toxoplasma gondii. Biochem. Soc. Trans. *20*, 296S.
18. Wang, Y., Hirata, T., Maeda, Y., Murakami, Y., Fujita, M., and Kinoshita, T. (2019). Free, unlinked glycosylphosphatidylinositols on mammalian cell surfaces revisited. J. Biol. Chem. *294*, 5038–5049.
19. Nakashima, M., Kashii, H., Murakami, Y., Kato, M., Tsurusaki, Y., Miyake, N., Kubota, M., Kinoshita, T., Saitsu, H., and Matsumoto, N. (2014). Novel compound heterozygous PIGT mutations caused multiple congenital anomalies-hypotonia-seizures syndrome 3. Neurogenetics *15*, 193–200.
20. Lam, C., Golas, G.A., Davids, M., Huizing, M., Kane, M.S., Krasnewich, D.M., Malicdan, M.C.V., Adams, D.R., Markello, T.C., Zein, W.M., et al. (2015). Expanding the clinical and molecular characteristics of PIGT-CDG, a disorder of glycosylphosphatidylinositol anchors. Mol. Genet. Metab. *115*, 128–140.
21. Tomavo, S., Couvreur, G., Leriche, M.A., Sadak, A., Achbarou, A., Fortier, B., and Dubremetz, J.F. (1994). Immunolocalization and characterization of the low molecular weight antigen (4-5 kDa) of Toxoplasma gondii that elicits an early IgM response upon primary infection. Parasitology *108*, 139–145.
22. Pagnamenta, A.T., Murakami, Y., Taylor, J.M., Anzilotti, C., Howard, M.F., Miller, V., Johnson, D.S., Tadros, S., Mansour, S., Temple, I.K., et al.; DDD Study (2017). Analysis of exome data for 4293 trios suggests GPI-anchor biogenesis defects are a rare cause of developmental disorders. Eur. J. Hum. Genet. *25*, 669–679.
23. Kawamoto, M., Murakami, Y., Kinoshita, T., and Kohara, N. (2018). Recurrent aseptic meningitis with *PIGT* mutations: A novel pathogenesis of recurrent meningitis successfully treated by eculizumab. BMJ Case Rep. *2018*. bcr-2018-225910. https://doi.org/10.1136/bcr-2018-225910.
24. Yang, L., Peng, J., Yin, X.-M., Pang, N., Chen, C., Wu, T.H., Zou, X.M., and Yin, F. (2018). Homozygous *PIGT* mutation lead to multiple congenital anomalies-hypotonia seizures syndrome 3. Front. Genet. *9*, 153.
25. Bayat, A., Knaus, A., Juul, A.W., Dukic, D., Gardella, E., Charzewska, A., Clement, E., Hjalgrim, H., Hoffman-Zacharska, D., Horn, D., et al.; DDD Study Group (2019). PIGT-CDG, a disorder of the glycosylphosphatidylinositol anchor: Description of 13 novel patients and expansion of the clinical characteristics. Genet. Med. Epub ahead of print. https://doi.org/10.1038/s41436-019-0512-3.
26. Knaus, A., Pantel, J.T., Pendziwiat, M., Hajjir, N., Zhao, M., Hsieh, T.C., Schubach, M., Gurovich, Y., Fleischer, N., Jäger, M., et al. (2018). Characterization of glycosylphosphatidylinositol biosynthesis defects by clinical features, flow cytometry, and automated image analysis. Genome Med. *10*, 3.
27. Gurovich, Y., Hanani, Y., Bar, O., Nadav, G., Fleischer, N., Gelbman, D., Basel-Salmon, L., Krawitz, P.M., Kamphausen, S.B., Zenker, M., et al. (2019). Identifying facial phenotypes of genetic disorders using deep learning. Nat. Med. *25*, 60–64.
28. Schroff, F., Kalenichenko, D., and Philbin, J. (2015). FaceNet: A unified embedding for face recognition and clustering. arXiv.
29. Pantel, J.T., Zhao, M., Mensah, M.A., Hajjir, N., Hsieh, T.-C., Hanani, Y., Fleischer, N., Kamphans, T., Mundlos, S., Gurovich, Y., and Krawitz, P.M. (2018). Advances in computer-assisted syndrome recognition and differentiation in a set of metabolic disorders. J. Inherit. Metab. Dis *41*, 533–539.
30. Reijnders, M.R.F., Janowski, R., Alvi, M., Self, J.E., van Essen, T.J., Vreeburg, M., Rouhl, R.P.W., Stevens, S.J.C., Stegmann, A.P.A., Schieving, J., et al. (2018). PURA syndrome: Clinical delineation and genotype-phenotype study in 32 individuals with review of published literature. J. Med. Genet. *55*, 104–113.
31. Ferry, Q., Steinberg, J., Webber, C., FitzPatrick, D.R., Ponting, C.P., Zisserman, A., and Nellåker, C. (2014). Diagnostically relevant facial gestalt information from ordinary photos. eLife *3*, e02020.
32. Brunner, H.G., and van Driel, M.A. (2004). From syndrome families to functional genomics. Nat. Rev. Genet. *5*, 545–551.

The American Journal of Human Genetics, Volume *105*

Supplemental Data

Mutations in *PIGU* Impair the Function of the GPI Transamidase Complex, Causing Severe Intellectual Disability, Epilepsy, and Brain Anomalies

Alexej Knaus, Fanny Kortüm, Tjitske Kleefstra, Asbjørg Stray-Pedersen, Dejan Đukić, Yoshiko Murakami, Thorsten Gerstner, Hans van Bokhoven, Zafar Iqbal, Denise Horn, Taroh Kinoshita, Maja Hempel, and Peter M. Krawitz

Supplemental Data

Clinical report of individuals with *PIGU*-associated GPIBD

Individual P-1, is the first daughter of healthy first-degree cousins. She was born after uncomplicated pregnancy at term with a birth weight of 3520 g (0.0 z, P 50), a birth length of 52 cm (0.02 z, P 51) and an occipitofrontal head circumference (OFC) of 33 cm (-2.00 z, P 2). APGAR score was 9/10/10 at one, five and ten minutes of life respectively. The first days of life were unremarkable, except phototherapy due to hyperbilirubinemia (max 27,3 mg/dl) at day four to six. Retrospectively parents noticed five to ten seconds of rhythmic myoclonic movements of the head, arms and less pronounced, the legs several times a day starting within the first month of life. At age three months, global developmental delay was documented. A first comprehensive examination took place at age seven months. The girl showed severe muscular hypotonia with reduced spontaneous movements, poor head control and inability to roll over. She interacted with reactive smiling, but she was not able to track objects with her eyes, to grasp or to make sounds. Tendon reflexes were weak except PSR. She showed repetitive myoclonic movements of the left hand and left leg. Measurements were within the normal range (weight 8.8 kg, 1.02 z, P 85; length 71 cm, 0.89 z, P 81; OFC 42 cm, -1.19 z, P 12). Electroencephalogram (EEG) revealed slowed basal activity, and polymorphic dysrhythmic delta waves with upstream high frequent sharp waves during sleep. MRI of the brain was unremarkable, as well as extensive metabolic work up. Eye examination revealed strabismus convergens at the age of one year. At age one year and 3 months she had still a severe global developmental delay, muscular hypotonia and persistent myoclonic seizures regardless of physiotherapy, early support and antiepileptic treatment. However, she could grasp and to roll over from back to belly. A second MRI of the brain revealed delayed myelination and a small periventricular focal gliosis on the left side. Reinforcement of antiepileptic therapy was able to reduce but not prevent seizures. At age two years she could roll over from back to belly and back, sit on all-fours positions and make sounds. Length and weight were normal, OFC was small (45.5 cm, -1.87 z, P 3). A further MRI of brain was normal except left sided periventricular gliosis.
Further course of disease was characterized by persistent focal myoclonic seizures up to 100 times a day, occurrence of generalized myoclonic-tonic seizures and the development of spasticity in all limbs leading to a slow regression and loss of all achieved skills. Due to dysphagia and dystrophy, a gastrostomy was implemented at age 8. Repeated extended metabolic analyses gave normal results except elevation of glutamine in plasma. A forth MRI of the brain at age 5 years showed atrophy of the white matter and an increase of lactate and a decrease of N-acetylaspartate (NAA) in the spectroscopy. X-ray of spine revealed osteopenia and scoliosis. Muscular biopsy was not suggestive for mitochondriopathy. Chromosomal analysis showed a normal female karyotype. Array-CGH revealed a 0,16Mb deletion in 11q14,1 (arr 11q14.1 (84,017,779-84,177,562)x1 (NCBI Build 36.1)), a CNV with unknown significance.

Individual P-2, a boy, is the third child of family 1 and the brother of individual P1. He was born at 41+3 weeks after normal pregnancy with normal measurements: birth weight of 3.5 kg (0.19 z, P42), birth length of 56 cm (1.44 z, P 93) and OFC of 37 cm (1.19 z, P 88) and good APGAR scores (9/10/10 at minute 1, 5 and 10 respectively). Parents reported normal postna-

tal adaptation and development in the first weeks of life. At the age of 7 weeks first generalized seizures occurred, followed by frequent focal myoclonic seizure series, which did not respond to different therapies. In the first weeks seizures were accompanied by apneas, but apneas occurred also independently and frequently required stimulation and oxygen insufflation. In addition to epilepsy severe muscular hypotonia and an insufficient eye contact were noted. Extended metabolic analyses at the age of two months gave normal results except a slight elevation of glutamine in plasma and glycoseaminoglycans (GAGs) in urine. EEG showed multifocal spikes and slow basal activity. ECG revealed an incomplete right bundle branch block (RBBB), and an ASD type II. Visual evoked cortical potentials (VECPs) were absent on the right eye and very small on the left eye. A fundoscopy of both eyes were inconspicuous as well as an MRI of brain. The development in the next years was poor. The boy did not achieve any milestones in motor development: he was never able to roll over, nor sit or walk. He never grasped. In toddlerhood he showed eye contact and he could follow with eyes, but these abilities were lost in the late preschool age. Optic atrophy was diagnosed at the age of 15 months. At age of 16 months acute hydrocephalus malresorptivus occurred requiring a placement of a ventriculo-peritoneal shunt system. Due to feeding difficulties the boy required PEG at age of three years. The boy was affected by recurrent upper airway infections which were often associated with an aggravation of seizures. At the age of 4 years he showed supraventricular tachycardia (heart frequency of 240/minute) for the first time, which was followed by further episodes of tachycardia requiring hospitalization and medical cardio version at different times.
Last examination took place at age of 10 years and 9 months. We saw a severe disabled boy with normal measurements (length 142 cm, -0.52 z, P 30; weight 35 kg, -0.42 z, P 34) who was not able to walk, sit unaided, nor to crawl or roll over. He had a severe truncal muscular hypotonia and hypertonia of all limbs. His spontaneous movements were very limited and he suffered from scoliosis. He gave sounds but did not speak syllables or words. He was blind due to severe optic atrophy. Feeding was completely by GI tube. Karyotyping revealed a normal male karyotype (46, XY). Array CGH revealed a 0,8Mb duplication in chromosome 5 (arr 5p15.33 (770,367-1,603,192)x3 (NCBI Build 36.1)) and a 0,16Mb deletion in 11q14,1 (arr 11q14.1 (84,017,779-84,177,562)x1 (NCBI Build 36.1)), both CNVs are of unknown clinical significance.

Individual P-3 was the first boy of non-consanguineous healthy parents of European descent (family 2), born at 42 weeks of gestation with a secondary caesarian section after a normal pregnancy with a birth weight 4.2 kg (1.18 z, P 88). He was hypotonic but there were no feeding problems. At 6 months of age he was examined by the ophthalmologist because of nystagmoid eye movements. At the age of 10 months he was admitted to the hospital because of pneumonia. One month later he had his first epileptic seizure. He presented with tonic and myoclonic seizures, thereafter mainly myoclonic seizures and absences treated with Valproate and Colbazam, but not fully controlled. A brain MRI showed progressive cerebellar atrophy. At the age of 6 years he showed dysmetric movement disorder. His height was 119.5 cm (0.31 z, P 62), weight was 20.5 kg (-0.38 z, P 35) and OFC was 53 cm (0.63 z, P 74). At this age he was not able to sit, stand or walk without help. He had no speech. There were no facial dysmorphisms noted. A variety of investigations followed including metabolic tests in blood, muscle biopsy and liquor, and genetic tests including chromosomal analyses, MLPA subtelomeric regions, genome wide array, DNA tests for *MECP2, FRAX, ATRX*, Pelizaeus-Mertzbacher *POLG, ARX, OPHN1*, mtDNA, all with normal results. He was followed in clinic regularly, at the age of 12 years he had no seizures during the daytime, and only at night a few times a week.

He was wheelchair bound, needed plasters for heel contractures, he had still not developed words and only used some sounds. His height was 144.5 cm (-1.03 z, P 15) and weight was 33.4 kg (-1.35z, P 9). At current age of 17 years he is a friendly boy and surgically corrected for his scoliosis.

Individual P-4 was the second boy of family 2 and the younger brother of P3, born at 39 weeks of gestation by primary SC after a normal pregnancy with a birth weight 4.7 kg (2.12 z, P 98). He was hypotonic and an MRI made at the age of 4 months showed frontal atrophy and a Dandy Walker variant. At the age of 8 months he was not able to roll. His length was 74 cm (0.73 z, P77), weight 9.4 kg (0.45 z, P 67) and OFC 49.5 cm (3.17 z, P 99). In general, his development was better than his brother. At the age of 5 years he was able to speak 2-3 word sentences and to walk few steps. His height at that age was 111.2 cm (-0.05 z, P 48), weight 18.5 kg (-0.26 z, P40) and OFC 53.2 cm (1.12 z, P 87). His first myoclonic seizures started at the age of 6 years which were generally well controlled with Levetiracetam. An MRI at this age showed progressive vermis hypoplasia. At the current age of 12 years he is a friendly boy, able to walk independently for short distances and to speak a few word sentences. He also developed scoliosis.

Individual P-5 was the first girl of non-con-sanguineous healthy parents of European descent (family 3), born at 42 weeks of gestation by normal delivery after a normal pregnancy with a birth weight 4.8 kg (2.70 z, P 99). She was hypotonic and had feeding problems right from the start. At the age of six weeks ophthalmologic examination revealed nystagmoid eye movements. At the age of three months she was admitted to the hospital due to poor head control and muscular hypotonia. EEG and brain MRI performed at the age of 5 months showed no pathological finding. A brain MRI performed at the age of 10 months showed a thin corpus callosum and an enhanced ventricular system without signs of hydrocephalus. At the age of 2 years she still showed hypotonia and general developmental delay. Her height was 91 cm (1.30 z, P 90), weight was 12.5 kg (0.35 z, P64) and OFC was 50.5 cm (1.84 z, P97). At this age she was not able to sit, stand or walk and she had no speech. Some facial dysmorphisms were noted, a broad forehead, a short and anteverted nose, a short philtrum and dysmorphic low set ears. A variety of investigations followed including metabolic tests in blood and liquor without pathological findings. Genome wide array-CGH results were negative. At the age of 3.5 years she developed focal onset seizures with impaired awareness and was successfully treated with Valproate.
She was followed in clinic regularly; at the age of 5 years she had no seizures. She was wheelchair bound and had developed only a few words and she is considered for a surgically corrected for her scoliosis. Her height was 116 cm (1.12 z, P 87), weight was 20 kg (0.04 z, P 66) and OFC was 53 cm (1.60 z, P 95).

Facial gestalt of individuals with *PIGU* mutations

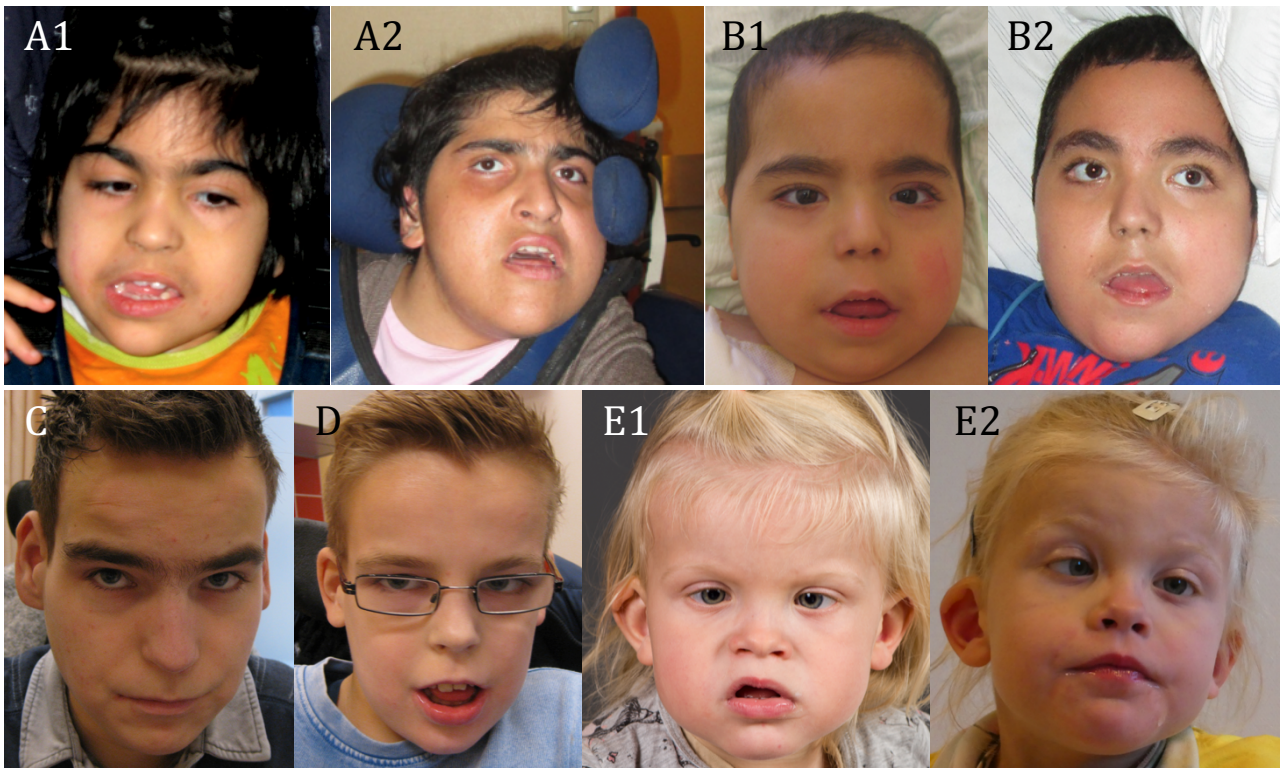

Figure S1. Facial appearance of individuals with biallelic PIGU-mutations. Individual P-1 at the age of 8 (A1) and 19 years (A2). Individual P-2 at the age of 3 (B1) and 12 years (B3). Individuals P-3 at the age of 17 years (C) and P-4 at the age of 12 years (D). Individual P-5 at the age 3 (E1) and 5 years (E2).

MRI of individuals with *PIGU*-associated GPIBD

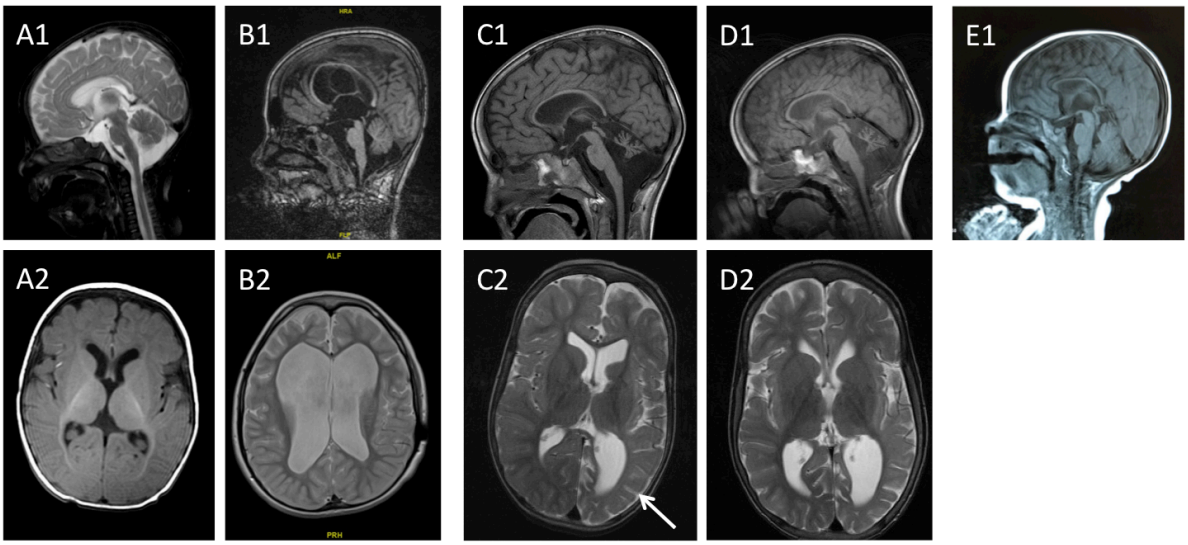

Figure S2. MRI scans of individuals with PIGU-associated GPIBD: MRI of individual P-2 at the age of 2 months was normal (A1, A2). At the age of 12 years he showed a hydrocephaly (B1, B2). MRI of individual P-3 revealed thin corpus callosum and vermis hypoplasia (C1) accompanied by asymmetric enlarged ventricles (left < right) and asymmetric myelinisation (C2, arrow) with no changes over time (D1, D2). MRI of individual P-5 showed a thin corpus callosum, vermis hypoplasia, and enlarged ventricles the age of 10 months (E1).

Clinical features of five individuals with *PIGU*-associated GPIBD

		Family 1		Family 2		Family 3
Individual		P-1	P-2	P-3	P-4	P-5
Genetic result	PIGU (NM_080476.4)	c.209T>A; p.Ile70Lys homozygous		c.1149C>A; p.Asn383Lys homozygous		c.1149C>A; p.Asn383Lys homozygous
Ethnicity		Turkish		European		Norwegian
Sex		Female	Male	Male	Male	Female
Genetic investigation		Sanger sequencing	WES	WES	WES	WES
Prenatal/ Neonatal						
Pregnancy		Normal	Normal	Normal	Normal	Normal
Birth at		40 weeks	40 weeks	42 weeks	39 weeks	42 weeks
Birth weight		3520 g/ P 54	3540 g/ P 35	4260 g/ P 84	4740 g/ P 98	4800 g/ >P 99
Birth length		52 cm/ P 56	56 cm/ P 94	Normal	Normal	50.5 cm/ P 19
Birth OFC		33 cm/ P 7	37c m/ P 86	Normal	Normal	37 cm/ P 90
Disease manifestation						
Age at manifestation of disease		First month	7 weeks	Birth	Birth	Birth
Presenting symptoms		Myoclonic seizures	Myoclonic seizure	Muscular hypotonia	Muscular hypotonia	Muscular hypotonia, feeding problems
Age at last examination		19 years	12 years	12 years	7 years	5 years
Weight at last examination		58 kg/ P 36	35 kg/ P 15	30.3 kg/ P 6	25.1 kg/ P 15	20 kg/ P 66
Length at last examination		155 cm/ P 2	142 cm/ P 5	146 cm/ P 6	124 cm/ P 50	116 cm/ P 87
OFC at last examination		Normal	Normal	Normal	Normal	53 cm/ P 95
Dysmorphic features						
		Malar flattening, smooth philtrum, thin upper lip, pointed chin, high arched palate, posteriorly rotated ears, hypertrichosis	Long face, high forehead, bitemporal narrowing, malar flattening, smooth philtrum, high arched palate, posteriorly rotated ears, hypertrichosis	Long face, high forehead, deep set eyes, long lose, malar flattening, smooth philtrum, thin upper lip	Long face, high forehead, malar flattening, smooth philtrum, thin upper lip	Broad forehead, epicanthus, telecathus, short nose, depressed nasal bridge, malar flattering, short philtrum, large mouth with downturned corners, low set dysplastic ears
Neurological features						
Developmental delay		Profound	Profound	Profound	Severe	Profound
Intellectual disability		Profound	Profound	Profound	Severe	Profound
Seizures		Yes	Yes	Yes	Yes	Yes
Seizure onset		1 months	2 months	10 months	6 years	3.5 years
Seizure characteristics		Initially focal myoclonic, now generalized	Generalized and focal myoclonic with apnoa	Myoclonic and absences, grand mal, tonic-clonic	Myoclonic	Focal
Seizure outcome		Intractable	Intractable	Relatively well controlled	Relatively well controlled	Well controlled
Muscular hypotonia		Yes	Yes	Yes	Yes	Yes, severe
Spasticity in limbs		Yes	Yes	No	No	No
Cortical visual impairment		Yes	Yes	No	No	Yes
Brain imaging						
Cerebral anomalies		Global cerebral atrophy	Hydrocephalus	Hydrocephalus	Frontal lobe atrophy	Slightly increased extracerebral fluid

Corpus callosum hypoplasia	No	Yes	Yes	No	Yes
Cerebellar atrophy/ vermis hypo-plasia	Cerebellar atrophy	No	Vermis and cerebellar hypoplaisa	Vermis hypoplasia, megacisterna magna	No
Neuronal migration defect	Delayed myelination	Delayed myelination	Focal abnormal gyri	Delayed myelination	No
Other	Increased lactate in spectroscopy	Hydrocephaly at age of 1 year	No	No	No
Ophthalmologic features					
Strabismus	Yes	Yes	Yes	Yes	Yes
Nystagmus	No	No	Yes	No	Yes
Hyperopia	No	No	No	Yes	Yes
Myopia	No	No	No	No	No
Other	-	Optic atrophy	-	-	-
Audiologic features					
Hearing loss	No	No	No	No	No
Cardiologic features					
Patent ductus arteriosus	No	No	No	No	No
Increased atrial load	No	No	No	No	No
Rhythm anomalies	No	Right bundle branch block, supraventricular tachycardia	No	No	No
Respiratory problems					
Recurrent infections	Yes	Yes	No	No	No
Gastro-intestinal problems					
Feeding problems	Yes, PEG tube	Yes, PEG tube	No	No	No
Urologic/Renal features					
Nephrocalcinosis	No	No	n.a.	n.a.	No
Urine calcium	Normal	Normal	n.a.	n.a.	No
Ureteral dilation	n.a.	No	No	No	No
Skeletal anomalies					
Slender long bones	Yes	Yes	No	No	n.a.
Scoliosis	Severe	Severe	Severe	Severe	Severe
Pectus excavatum	No	No	No	No	Yes
Joint hypermobility	No	No	No	No	Yes
Osteopenia	Yes	n.a.	n.a.	n.a.	n.a.
Blood and CSF analysis					
Plasma alkaline phosphatase	Normal	Normal	Normal	Normal	Normal
Plasma calcium	Normal	Normal	Normal	Normal	Normal
Plasma phosphate	Normal	Normal	Normal	Normal	Normal
Parathyroid hormone values	n.a.	Normal	n.a.	n.a.	n.a.
Hypertriglyceridemia	No	No	No	No	No
CSF analysis	Normal	Normal	Normal	Normal	Normal
CSF albumin & albumin quotient	n.a.	n.a.	Normal	Normal	Normal

Abbreviation:
n.a. not analyzed
PEG: Percutaneous endoscopic gastrostomy
WES: Whole exome sequencing

Methods:

Multicolor flow cytometry

Blood samples of affected individuals, parents and healthy unrelated controls were collected in BCT CytoChex (Streck®) tubes. Erythrocytes from 50µl blood were removed using hypo-osmotic lysing buffer. The cells were washed and stained with fluorescently labeled antibodies against a cluster of differentiation (CD) marker for cell population gating (CD45 and CD19) and GPI-APs (CD16, CD24, CD55, and CD59), as well as with fluorescein-labeled proaerolysin (FLAER), which binds to the GPI anchor itself. Detection of free GPI anchors was accomplished using T5 4E10 antibody[1–3] and AF647 labed anti-IgM secondary antibody. The antibody stating was incubated for 30 min at room temperature, cells were washed in excess of flow cytometry buffer and re-suspended in 250µl FACS buffer for analysis on a MACSQant VYB (Miltenyi Biotec). Gating for living cells was based on forward and side scatter (FSC-A vs. SSC-A). Single cells were gated on a diagonal (FSC-A vs. FSC-H). Granulocytes were identified as granular (SSC-A high) and CD45-positive cells, B-cells as non-granular (SSC-A low) and CD19-positive cells. Flow cytometry data analysis was carried out using FlowJo V9.66 and Microsoft Excel.

The relative change of GPI-AP expression was determined by a ratio of the staining index (SI) of a patient to the SI of healthy controls (parents or unrelated individuals): The SI is calculated as the ratio of median fluorescent intensity (MFI) of a stained cell population (MFI_{pos}) minus the MFI of unstained (or antibody isotype control stained) cell population (MFI_{neg}) to twice the standard deviation of MFI_{neg}.

Functional analysis of p.Asn393Lys variant in *PIGU* by flow cytometry in CHO cells

PIGU deficient CHO cell (C311PA16)[4] were transiently transfected with wild type or mutant (p.Asn383Lys) pMEhPIGU-FLAG. Restoration of the surface expression of CD59, DAF, and urokinase plasminogen activator receptor (uPAR), were assessed 2 days later by flow cytometry. Wild-type PIGU efficiently restored the surface expressions of CD59, DAF, and uPAR whereas p.Asn383Lys mutant rescued less efficiently (Figure S3 A). Experiments were performed in duplicates.

Lysates from transfectants in Figure S3 A were applied to SDS PAGE and western blotting were performed. Mutant PIGU expression was similar compared to wild type protein, normalized by the intensity of GPADH as loading control. Luciferase acitivity was used for evaluation of transfection efficiency (Figure S3 B).

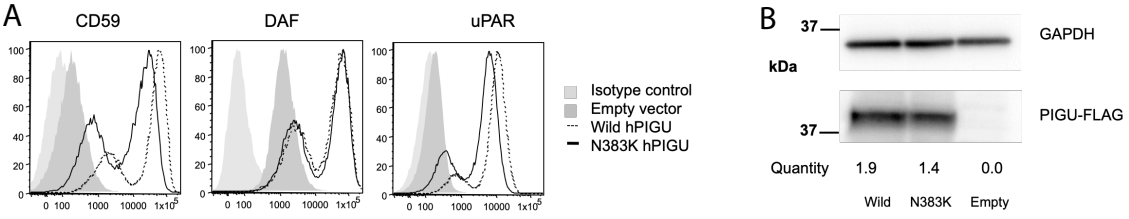

Figure S3. Functional analysis of p.Asn383Lys mutation in PIGU. (A) Restoration of CD59, DAF, and uPAR expression after transient transfection of *PIGU* deficient CHO cell lines. Grey shadow, empty vector; light grey shadow, isotype control. (B) Western blot analysis of p.Asn383Lys mutant and wild type PIGU of transiently transfected PIGU deficient CHO cells.

Facial Analysis

Frontal facial images of the five individuals with PIGU mutations were collected with informed consent of their parents or legal guardians. 128-dimensional facial embeddings vectors for each of the 112 patients (25 PIGA, 15 PIGN, 13 PIGT, 5 PIGU, 5 GPAA1, 24 PIGV, and 25 PGAP3 cases) were extracted using a pre-trained FaceNet model[5] (version 20170512-110547). The similarity of faces correlates with the distance between facial embeddings after an L2 norm (Euclidean norm) is calculated. In order to compare the faces in a gene cohort manner, the facial embeddings of four random samples from a gene cohort were selected and averaged to generate one self-reference point. The four facial embeddings were removed from the gene cohort and the process was iterated. When less than four embeddings remained for a gene cohort, all former embeddings were added. This process was iterated over the number of samples present in each gene cohort (4*25 for PIGA, 4*15 for PIGN, 4*13 for PIGT, 4*5 for PIGU, 4*5 for GPAA1, 4*24 for PIGV, and 4*25 for PGAP3) yielding 448 self-reference points that form the GPIBD space. In order to represent the position of each patient in the GPIBD space, Euclidean distances from all cases to all the self-reference points were computed. Only the shortest distance between all self-reference points for a gene was considered, thus the final distance matrix contains seven distance values representing each case. Thereafter, the centroids for each gene cohort were calculated and the Euclidean distances between the centroids were computed and hierarchically clustered using the single linkage method (Figure 5).

References

1. Azzouz N, Shams-Eldin H, Niehus S, et al. Toxoplasma gondii grown in human cells uses GalNAc-containing glycosylphosphatidylinositol precursors to anchor surface antigens while the immunogenic Glc-GalNAc-containing precursors remain free at the parasite cell surface. *Int J Biochem Cell Biol*. 2006;38(11):1914-1925. doi:10.1016/j.biocel.2006.05.006.
2. Hirata T, Mishra SK, Nakamura S, et al. Identification of a Golgi GPI-N-acetylgalactosamine transferase with tandem transmembrane regions in the catalytic domain. *Nat Commun 2018 91*. 2018;9(1):405. doi:10.1038/s41467-017-02799-0.
3. Striepen B, Tomavo S, Dubremetz JF, Schwarz RT. Identification and characterisation of glycosyl-inositolphospholipids in Toxoplasma gondii. *Biochem Soc Trans*. 1992;20(3):296S.
4. Hong Y, Ohishi K, Kang JY, et al. Human PIG-U and Yeast Cdc91p Are the Fifth Subunit of GPI Transamidase That Attaches GPI-Anchors to Proteins. Guidotti G, ed. *Mol Biol Cell*. 2003;14(5):1780-1789. doi:10.1091/mbc.E02-12-0794.
5. Schroff F, Kalenichenko D, Philbin J. FaceNet: A Unified Embedding for Face Recognition and Clustering. March 2015. doi:10.1109/CVPR.2015.7298682.